Earth and Planetary Science Letters 301 (2011) 337–344

Contents lists available at ScienceDirect

Earth and Planetary Science Letters

journal homepage: www.elsevier.com/locate/epsl

Acceleration and evolution of faults: An example from the Hunter Mountain–Panamint Valley fault zone, Eastern California

Noel Gourmelen *[,1], Timothy H. Dixon, Falk Amelung, Gina Schmalzle [2]

University of Miami, USA

ARTICLE INFO

Article history:
Received 21 April 2009
Received in revised form 1 November 2010
Accepted 7 November 2010
Available online 3 December 2010

Editor: R.D. van der Hilst

Keywords:
geodesy
fault evolution
InSAR
rock mechanics
Western United States
Eastern California Shear Zone
Hunter Mountain Fault

ABSTRACT

We present new space geodetic data indicating that the present slip rate on the Hunter Mountain–Panamint Valley fault zone in Eastern California (5.0 ± 0.5 mm/yr) is significantly faster than geologic estimates based on fault total offset and inception time. We interpret this discrepancy as evidence for an accelerating fault and propose a new model for fault initiation and evolution. In this model, fault slip rate initially increases with time; hence geologic estimates averaged over the early stages of the fault's activity will tend to underestimate the present-day rate. The model is based on geologic data (total offset and fault initiation time) and geodetic data (present day slip rate). The model assumes a monotonic increase in slip rate with time as the fault matures and straightens. The rate increase follows a simple Rayleigh cumulative distribution. Integrating the rate-time path from fault inception to present-day gives the total fault offset.

1. Introduction

The processes and rates of fault zone evolution are poorly understood, but have important implications for the mechanical nature of faults, seismic process and hazard, and regional tectonics. Fault slip rates averaged over different time spans may help define and perhaps understand this evolution. However, before this can be realized, we need to better understand the various sources for discrepancies between rates spanning different times. For large offset, mature fault zones such as the Carizo segment of the San Andreas fault in central California, geodetic rates averaged over decadal time scales, and geologic rates over longer time scales, are usually very similar (Dickinson, 1996; Lisowski et al., 1991; Liu-Zeng et al., 2006; Meade and Hager, 2005; Schmalzle et al., 2006; Sieh and Jahns, 1984). However, for other fault zones, discrepancies between geodetic and geologic rates are often observed, and have led to suggestions of complex behavior such as slip pulses, strain waves, and possible relations to earthquake clusters and other non-linear spatial-temporal deformation processes (Bennett et al., 2004; Dolan et al., 2007; Friedrich et al., 2004; Marco et al., 1996; Meade and Hager, 2005; Oskin and Iriondo, 2004; Oskin et al., 2008; Peltzer et al., 2001; Rockwell et al., 2000).

There are additional confounding factors. For example, geological rate estimates are minimum estimates, because the feature used to define fault offset formed some unknown time prior to fault initiation. These rates therefore tend to be slower than geodetic estimates. On the other hand, geodetic estimates are model-dependant, requiring some knowledge of crustal rheology and earthquake history before the near-field strain rates can be used to estimate a reliable far field (i.e. long term) slip rate. Errors in the input model can lead to biased rate estimates (Dixon et al., 2003; Johnson et al., 2007).

Another explanation for discrepancies between geologic and geodetic rates may apply to some young fault zones, (i.e., those which have not reached a steady-state slip rate). A new fault by definition must experience a finite period of acceleration, during which rate differences over different time spans are expected. However, it has been difficult to document this phenomenon due largely to data limitations. A rigorous definition of mature and immature faults is also lacking.

Here we present new space geodetic data describing recent motion across the Hunter Mountain–Panamint Valley fault zone, one of several active fault zones within the Eastern California Shear Zone (Fig. 1). We interpret our geodetic results in the context of newly available constraints on the initiation age of the Hunter Mountain fault (Lee et al., 2009). Our data indicate that present-day motion across the Hunter Mountain fault is significantly faster than available

* Corresponding author. School of Earth and Environment, University of Leeds, Leeds, LS2 9JT, UK. Tel.: +44 113 343 9085.
E-mail address: n.gourmelen@leeds.ac.uk (N. Gourmelen).
[1] Now at the University of Leeds, UK.
[2] Now at the University of Washington, USA.

0012-821X/$ – see front matter © 2010 Elsevier B.V. All rights reserved.
doi:10.1016/j.epsl.2010.11.016

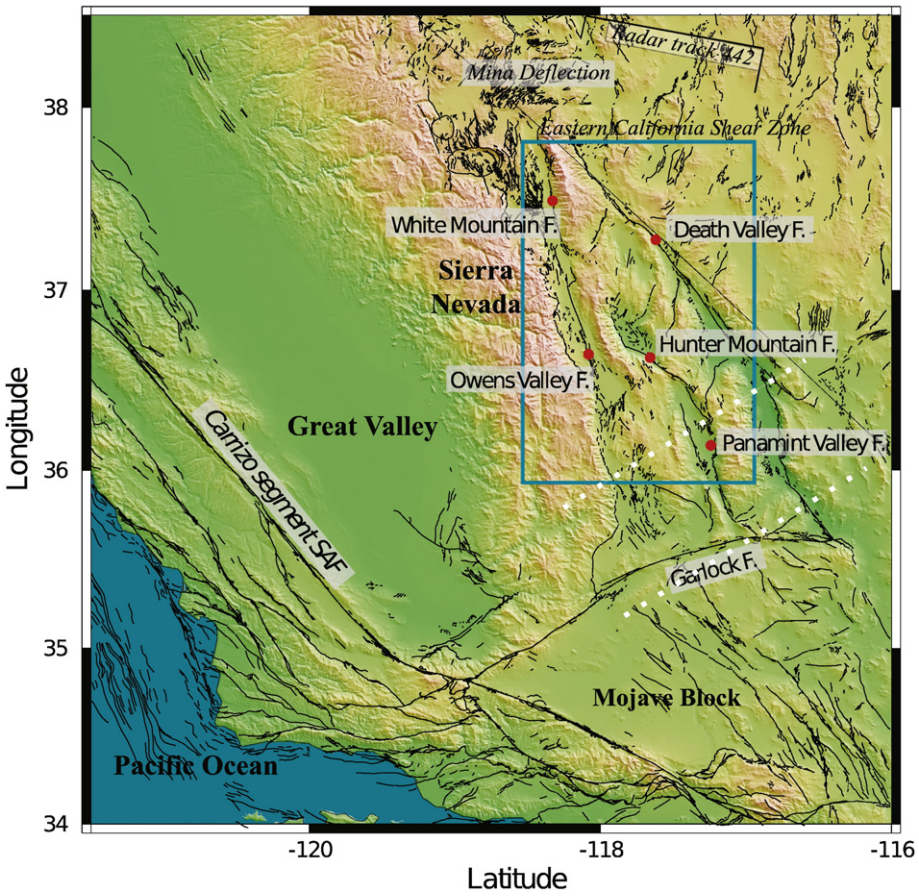

Fig. 1. Map of major geological features in study area. Red dots indicate location of named fault, FZ is fault zone, SAF is San Andreas Fault. Blue box: location of Figure 3a. "Radar Track 442" indicates location of InSAR data in Figures 3. The two white dashed lines mark the southern and northern limits of the GPS used in our analysis. The faults are from the USGS Quaternary fault database (U.S. Geological Survey, New Mexico Bureau of Mines and Mineral Resources and Nevada Bureau of Mines and Geology, 2006). The map has been created using the SRTM topography.

geologic estimates. We suggest that this is a consequence of the fault's relative youth, and slip acceleration over the last few million years. Our findings have important implications for understanding the time scales and processes by which faults straighten and simplify with time, and for interpretation of fault slip rate data and some rate discrepancies.

2. Geologic background and previous work

The Eastern California Shear Zone (ECSZ) represents a zone of significant right lateral shear in western North America, accommodating ~20–25% of Pacific-North America motion (Bennett et al., 2003; Dixon et al., 2000; Dokka and Travis, 1990a,b; Frankel et al., 2007; Lee et al., 2009; Miller et al., 2001; Sauber et al., 1994; Savage et al., 1990) (Fig. 1). Most of the remaining motion is accommodated by the San Andreas Fault. North of the Garlock fault and south of the Mina deflection, the ECSZ represents the eastern boundary of the rigid Sierra Nevada block, accommodating northwest translation of the block relative to the interior of the Basin and Range, presumably in response to northwest Pacific plate motion (Dokka and Travis, 1990b). In this region, the ECSZ includes three and perhaps four active, subparallel fault zones: the Owens Valley–White Mountain fault zone to the west, the Death Valley–Furnace Creek–Fish Lake Valley fault zone to the east, and the central Hunter Mountain–Panamint Valley fault zone, the focus of this study (Fig. 1). The State Line fault, east of the Death Valley–Furnace Creek fault zone, may also be active, accommodating a small amount of motion at present, although it has been more active in the past (Guest et al., 2007).

The ECSZ is a relatively young feature, and is an excellent "natural laboratory" for studying fault initiation and evolution; Dokka and Travis (1990a,b) estimated that ECSZ activity began in the eastern Mojave Desert between about 6 Ma and 10 Ma. Wernicke and Snow (1998) document a change in Sierra Nevada motion relative to stable North America, from westerly between 16 Ma and 10 Ma, to northwest or north–northwest beginning about 10 Ma, presumably marking the initiation of ECSZ motion. Atwater and Stock (1998) document a change in Pacific plate motion relative to North America at around 8 Ma, from WNW to NW. Reheis and Sawyer (1997) suggest that right lateral motion on the Fish Lake Valley fault, the northern continuation of the Death Valley–Furnace Creek fault zone, also began about 10 Ma (bracketed between 11.9 Ma and 8.2 Ma). Stockli et al (2003) place the initiation of strike slip motion in Fish Lake Valley at 6 Ma. All of these studies are thus broadly consistent with initiation of the ECSZ between about 6 Ma and 10 Ma. Du and Aydin (1996) suggest that the ECSZ acts as a "strain bypass" related to formation of the Transverse Ranges and the "big bend" of the San Andreas fault, associated with the inland jump of the plate boundary to its current position in the Gulf of California beginning about 5.5 Ma (Atwater, 1989; Oskin et al., 2001). Hence ECSZ activity may have accelerated after 5.5 Ma.

Pacific–North America plate motion has remained essentially constant for the last few million years (DeMets and Dixon, 1999; Sella et al., 2002). This represents the kinematic boundary condition for the ECSZ. However, significant rate differences for different time intervals are possible for individual ECSZ faults. Faults within the ECSZ are constantly evolving, perhaps in response to westward migration of the shear zone (Calzia and Ramo, 2000; Dixon et al., 1995; Dokka

and Travis, 1990a; Dokka and Travis, 1990b; Jones et al., 2004; McQuarrie and Wernicke, 2005; Stockli et al., 2003).

Initiation age, total offset and geologic rate

The Hunter Mountain fault is kinematically linked to more northerly striking normal faults to the north (Saline Valley fault zone, bounding the east side of the Inyo Mountains) and south (Panamint Valley fault, bounding the east side within Panamint Valley, and Ash Hill fault, within the valley, Fig. 1). The age of fault initiation is bracketed between 2.8 Ma and 4.0 Ma (Burchfiel et al., 1987; Hodges et al., 1989; Lee et al., 2009). The 4.0 Ma age represents the youngest age of Pliocene basalts offset by the fault; fault initiation is reckoned to occur sometime after basalt eruption. The basalts are not found in low-lying Panamint Valley, but only on surrounding hills, and hence erupted prior to valley formation. More recent work (Lee et al., 2009) suggests a 2.8 Ma initiation age, based on zircon and apatite U–Th/He thermochronometry from the east side of the Inyo Mountains. These data indicate more rapid uplift and exhumation of the Inyo Mountains after 2.8 Ma, suggesting initiation of the Saline Valley fault (and by implication the Hunter Mountain–Panamint Valley fault zone) at that time. We use this age in the subsequent discussion.

The total offset of the Hunter Mountain fault can be estimated from offset of the Hunter Mountain pluton, the width of Panamint and Saline Valleys in a direction parallel to the Hunter Mountain fault, and piercing points associated with Miocene–Pliocene age basaltic volcanics that ring northern Panamint Valley. A widely quoted estimate (9.3 ± 1.4 km; (Burchfiel et al., 1987; Sternloff, 1988)) is based on the intersection of the steep southeastern contact of the Hunter Mountain batholith and the nearly horizontal unconformity at the base of Miocene–Pliocene volcanics; displacement of this feature across the Hunter Mountain fault is mainly horizontal, consistent with strike slip motion.

Published geologic slip rates for the Hunter Mountain–Panamint Valley fault are of two types. First, detailed studies of offset alluvial fans and young drainage channels allow definition of Pleistocene or Holocene-averaged rates, ranging from 2.4 to 4 mm/yr (Oswald and Wesnousky, 2002; Zhang et al., 1990). Second, long term average rates defined over the entire time span of fault activity are defined by dividing total offset (9.3 km) by the fault initiation age. Using the most recently published age (2.8 Ma) Lee et al. (2009) obtain 3.3 ± 1.0 mm/yr. This rate by definition is less than the present day rate if the fault is accelerating (Fig. 2). In general, we expect that geologic rates averaged over Holocene time should be similar to present day geodetic rates, unless complex temporal behavior, or earthquake cycle effects bias the geodetic measurement (Dixon et al., 2003; Johnson et al., 2007), or if the fault is spatially complex and some deformation is missed in the geologic study (Lee et al., 2001). South of the Hunter Mountain fault, deformation may be partitioned between the Panamint Valley fault, a shallow, west dipping oblique slip fault that crops out on the east side of the valley, and more steeply dipping or vertical right lateral strike slip faults to the west, within the valley, such as the Ash Hill fault (Densmore and Anderson, 1997; Walker et al., 2005). Geologic studies on individual faults in Panamint Valley may therefore yield rates that are low compared to the entire deforming zone that includes the paired normal fault — strike slip fault system, or to the Hunter Mountain fault to the north, where deformation is more focused (Fig. 3a).

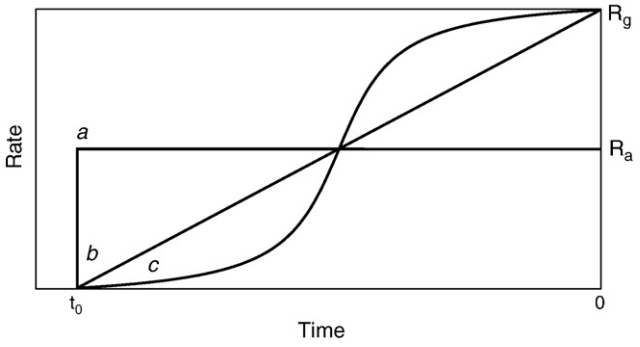

Fig. 2. Three conceptual rate-time paths for a young, accelerating fault, all with the same total offset, defined by the integral of the rate-time function (area under the curves). R_g is the geodetic rate, R_a is the average rate since fault inception. In cases *b* (linear growth) and *c* (Rayleigh growth), R_g is exactly twice as fast as R_a, while in case *a* (instantaneous growth), R_a and R_g are equal. Knowledge of R_g, age and total offset provides a way of distinguishing among the different growth models.

3. Space geodetic data

We processed 44 Synthetic Aperture Radar (SAR) images from the European Space Agency satellites ERS1/2 acquired between 1992 and the end of 2000 to produce a ground velocity map in the radar line-of-sight direction (LOS) spanning most of the ECSZ (Gourmelen et al., 2010). SAR Interferometry (InSAR) data has been used in a number of tectonic studies, including measurement of co-seismic (Massonnet et al., 1993), interseismic (Fialko, 2006), and postseismic (Gourmelen and Amelung, 2005) deformation. In this paper, we apply the Small BAseline Subset (SBAS) Interferometry technique to obtain a time series of ground displacement. The SBAS technique has been widely applied in the last few years (Berardino et al., 2002; Gourmelen et al., 2007; Lanari et al., 2004; Lundgren et al., 2001). SBAS relies on multiple (in this case more than a hundred) conventional interferograms with small spatial and temporal baseline, reducing long spatial wavelength noise, and allowing investigation of low slip rate faults. Details of the processing approach can be found in Gourmelen et al. (2010). The linear least squares component of the time series (analogous to a stack of the time series) is shown in Figure **3**a. The corresponding velocity profile across the Hunter Mountain fault is shown in Figure 3b.

We also process available GPS data in the region, generating an independent surface velocity profile for comparison to the InSAR data. We use the GPS velocity field of Schmalzle (2008) that is composed of continuous and campaign GPS data in the Western United States provided by Southern California Earthquake Center (SCEC), Basin and Range GPS Network (BARGN), Southern California Continuous GPS Network (SCIGN), Plate Boundary Observatory (PBO) GPS network, the United States Geologic Survey (USGS), and the University of Miami Geodesy Lab (UMGL). Data span from 1994 to 2008. A subset of data are used in a formal inversion procedure (Ward, 1990) to derive site velocities relative to the Central Basin and Range (see Table 5.2 in Schmalzle (2008)) which is believed to be relatively stable compared to areas to the east and west (Dixon et al., 1995) and provide a geologically reasonable reference to discuss ECSZ velocities. All sites in the subset are continuous with a minimum of 2.3 years of data collected but most sites have at least 8 years. Velocities with respect to the Central Basin and Range progressively increase from east to west, with the largest velocity gradient in the ECSZ west of the Panamint Valley–Hunter Mountain fault trace (Schmalzle, 2008). A GPS velocity profile across the Panamint Valley portion of the fault, about 30 km south of the InSAR profile, is shown in Figure 4.

4. Models for fault slip rate evolution

Pioneering analogue experiments in clay- and sandbox models by Tchalenko (1970) first demonstrated the tendency of faults to simplify with time, with initial offset accommodated by highly distributed deformation, and overall slip resistance decreasing with increasing offset as the fault zone becomes focused on a central, narrow shear zone. On a similar spatial scale, Bodin et al. (1994) showed that creepmeter measurements of slip amplitude were generally larger than measured feature offsets, even when the creepmeter spanned just a few meters on either side of the active

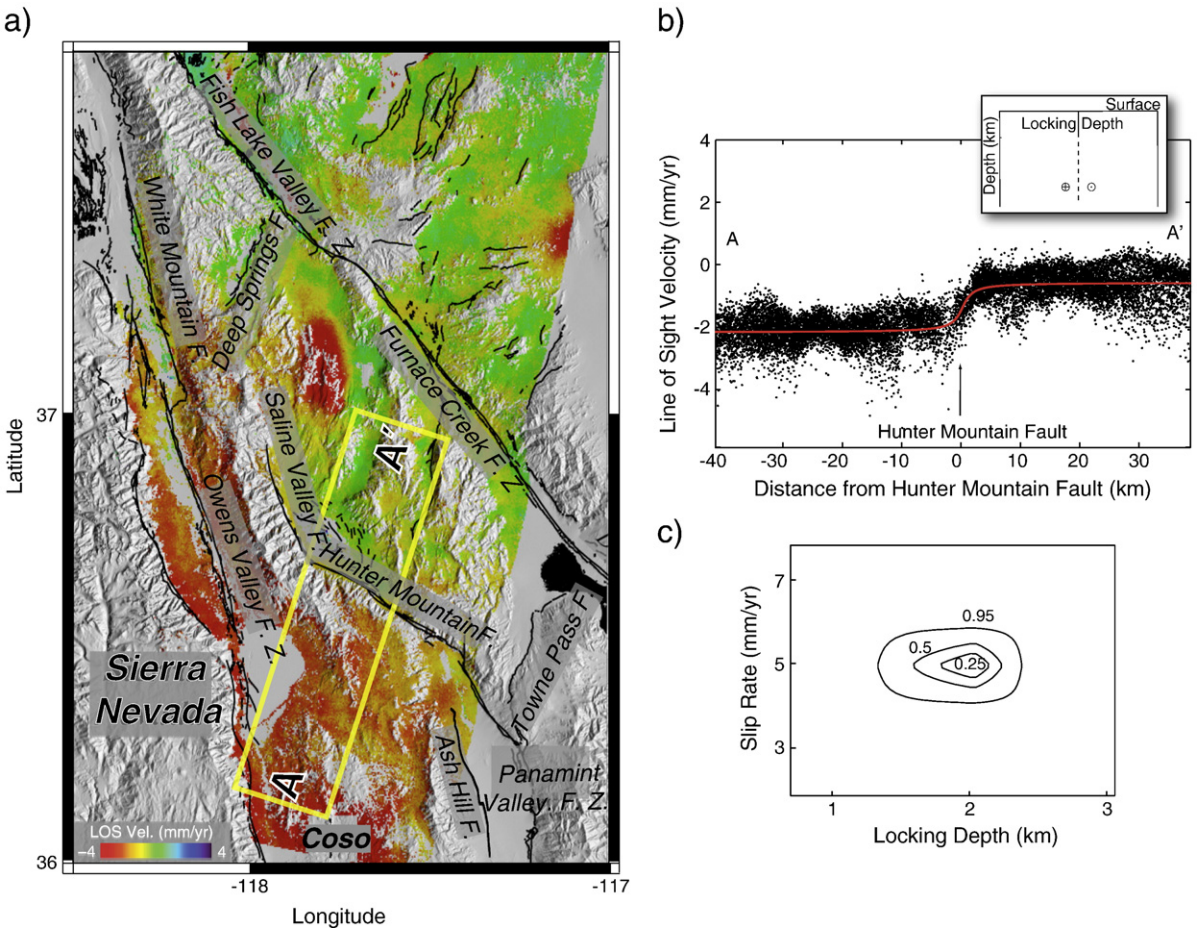

Fig. 3. InSAR surface displacement map and fault slip rate modeling for the Hunter Mountain fault (modified from Gourmelen et al. (2010)) a) InSAR based Line of Sight (LOS) velocity map for the ECSZ, based on data acquired between 1992 and 2000. Red oval marks coseismic plus post-seismic displacement associated with the 1993 M 6.1 Eureka Valley earthquake (Peltzer and Rosen, 1995). Yellow box shows location of profile in Figure 3b. F is Fault, FZ is Fault Zone. Faults are from the USGS quaternary fault database (U.S. Geological Survey, New Mexico Bureau of Mines and Mineral Resources and Nevada Bureau of Mines and Geology, 2006). b) Line Of Sight displacement along A–A′ (Fig. 3a). Strain accumulation model in red, assuming a vertical fault, with locked (solid line) and freely slipping (dashed line) segments (inset). Note high strain rate near fault, corresponding to shallow locking depth. Best-fit slip rate is 4.9 ± 0.8 mm/yr assuming pure strike slip in the strike direction of Hunter Mountain Fault. c) Model parameters (Brooks and Frazer, 2005), for the model in Figure 3b showing tradeoff between slip rate and locking depth. Unlike models with deeper locking depth, there is little tradeoff between slip rate and locking depth.

fault strand. On the scale of a single fault segment, Fialko et al. (2005) note that the immature fault associated with the Bam earthquake has a significant co-seismic slip deficit in the upper crust compared to slip at depth, attributed to distributed deformation in the upper few km of crust. Bennett et al. (1995) note a similar upper crustal slip deficit for the 1992 M 6.1 Joshua Tree earthquake, at the southern end of the ECSZ. On the scale of multi-segment fault zones, aftershock distributions associated with the Landers earthquake in the Mojave Desert (Liu et al., 2003) and paleoseismic work in the Central Nevada Seismic Belt (Bell et al., 2004) illustrate the tendency of immature faults to exhibit multiple overlapping or en-echelon active fault strands. With time, as total offset increases, these faults will presumably simplify their geometry (Wesnousky, 1988).

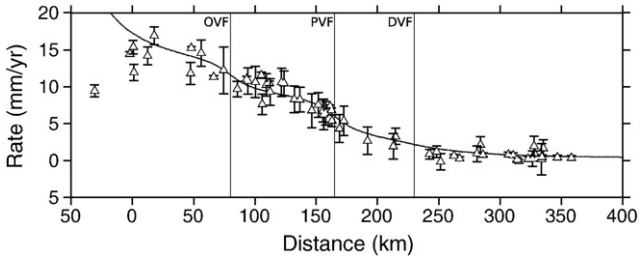

Fig. 4. GPS profile, perpendicular to the plate motion direction, across the Owens Valley fault (OVF), Panamint Valley fault (PVF), and the Death Valley fault (DVF), GPS velocities relative to central Basin and Range. GPS location is indicated by dashed lines on Fig. 1. The solid line is a best-fit viscoelastic coupling model. Modified from Schmalzle (2008).

Fault zone evolution from the beginning of a fault's active period to "middle age" may be described in terms of slip rate as a function of time, with the fault beginning at a condition of zero offset and zero slip rate. Offset and slip rate then increase until steady state is reached, whereafter offset increases at a uniform rate and slip rate remains constant. Figure 2 presents three simple possible models of slip rate evolution leading to similar total offset but different slip rate histories. Through geodetic data we can infer the present day rate, and geological data can give rates averaged over various time intervals, in principle placing some constraints on the rate-time path. Few studies have considered the fact that, for faults in which initiation age is known, the three key data defining fault evolution (present rate, total offset, and initiation age) are not independent: the integral of a given rate-time path, beginning at zero rate at fault initiation age, and ending with the present-day rate, yields the total fault offset. If the latter parameter is known from geologic studies, then integrating possible rate-time paths provides a useful (though non-unique) model test.

A simple Rayleigh cumulative distribution provides a conceptually simple model for non-linear fault evolution with some physical basis. The Rayleigh distribution is a subset of the Weibull distribution, often used to model failure in complex systems, including fracture

propagation in brittle materials (Kurth and Cox, 1985). The Rayleigh distribution is the simplest Weibull distribution, defined by a single parameter, S, the Rayleigh scale parameter. We imagine that prior to fault development, a large number of randomly oriented pre-existing fractures exist in the upper crust. As the proto-fault is stressed, the probability of these fractures slipping initially increases. As this occurs, properly oriented fractures fail repeatedly and lengthen, eventually coalescing to produce a through-going fault. At this point, overall stress is reduced, decreasing the probability of additional fractures being exploited. The rate of fracture exploitation follows a Rayleigh distribution, increasing rapidly from the fault initiation time, with a peak determined by S, and then decaying. Fault slip rate is related to the cumulative displacement on the individual fractures, initially increasing rapidly, and then more slowly, finally reaching a constant maximum rate. Hence the fault slip rate as a function of time, $R(t)$, follows a cumulative Rayleigh distribution, scaled by the stationary (final) rate, R_f:

$$R(t) = R_f\left[1-e^{\frac{-(t-t_0)^2}{2S^2}}\right] \quad (1)$$

The slip rate is zero at $t=t_0$, increasing monotonically to R_g at $t=0$ (t is reckoned negative before present). At $t=0$, the present day geodetic rate R_g is:

$$R_g = R_f\left[1-e^{\frac{-(t_0)^2}{2S^2}}\right] \quad (2)$$

Eq. (1) then becomes:

$$R(t) = R_g\frac{1}{1-e^{\frac{-(t_0)^2}{2S^2}}}\left[1-e^{\frac{-(t-t_0)^2}{2S^2}}\right] \quad (3)$$

S is the time of peak acceleration of slip rate and can be estimated from the known total fault offset by integrating Eq. (3). At this time the rate, R_s is close to one half its final value, and accumulated offset is D_s.

5. Geodetic slip rates

The new InSAR data document a remarkable zone of high velocity gradient across the Hunter Mountain fault. In contrast, most other active ECSZ faults imaged in this data set exhibit low velocity gradients in the immediate vicinity of the fault, consistent with strain accumulation patterns around faults with larger locking depths of 10–20 km, the typical range of locking depths in this region (McClusky et al., 2001; Meade and Hager, 2005; Miller et al., 2001). For a series of sub-parallel strike slip faults that are relatively closely spaced, the corresponding overlapping strain fields have made it challenging to estimate independent slip rates from geodetic data; while the summed slip rate across the entire shear zone is well constrained, the individual fault rates are not. Because of this high velocity gradient (and the implied shallow locking depth), the new InSAR data provide an opportunity to estimate the velocity of the Hunter Mountain fault, independent of the strain effects from the adjacent Owens Valley and Death Valley–Furnace Creek fault zones.

While areas to the south (Panamint Valley) and north (Saline Valley) of the Hunter Mountain fault undergo oblique slip with a component of extensional motion, the section of the fault imaged by InSAR is believed to be a simple strike slip fault with little vertical motion. We assume a simple strike slip fault model with no vertical motion, converting the satellite LOS range change (a scalar quantity) into purely horizontal motion. We then use a simple elastic screw dislocation model (Weertman and Weertman, 1964; Savage and Burford 1973), and solve for best fitting slip rate (4.9 ± 0.8 mm/yr) and locking depth (2 ± 0.4 km) (Fig. **3**c; Gourmelen et al., 2010); the error estimate represents the 2-sigma interval. The data are well fit with this simple model, and no distributed deformation or additional faults are indicated.

Further south, across the Panamint Valley fault, we determine the Panamint fault slip rate from the GPS dataset using a coupling model, with an elastic layer over a viscoelastic half space (Savage and Lisowski, 1998). This model explicitly accounts for earthquake cycle effects for the San Andreas, Owens Valley, Panamint Valley and Death Valley faults and the ductile rheology of the lower crust/upper mantle to a first approximation. Model parameters are listed in Table 1, details are given in Schmalzle (2008). The GPS determined fault slip rate is 5.1 ± 0.5 mm/yr of fault-parallel motion, with negligible fault-normal motion.

The GPS rate is essentially identical to the InSAR-based estimate; hereafter we use the linear combination of the two estimates (5.0 ± 0.5 mm/yr). This rate is significantly faster than available geologic estimates, including the Holocene estimate (Lee et al., 2009; Oswald and Wesnousky, 2002) at 95% confidence (Fig. 5). While the uncertainties for the geologic estimates may be underestimated (Zechar and Frankel, 2009), there does appear to be a systematic difference between all the available geologic estimates and the new geodetic estimates.

6. Geodetic locking depth

The shallow locking depth across the Hunter Mountain fault is highly unusual, and we lack a good explanation. Perhaps it is related to the elevated geothermal gradient associated with the nearby Coso geothermal field (Fig. 3a; Gourmelen et al., 2010). Monastero et al (2005) suggest that Coso represents a nascent metamorphic core complex, with a significant shallowing of the brittle-ductile transition, a mechanical boundary in the crust closely related to locking depth. Alternately, it may reflect the kinematics of the Hunter Mountain Fault, which can be considered a short transfer fault linking oblique-extensional low angle normal faults to the north (Saline Valley) and south (Panamint Valley). The Panamint Valley fault is inferred to have a very shallow decollement depth (less than 1 km) based on the depth of alluvial fill in the valley (Burchfiel et al., 1987; Hodges et al., 1989). This shallow decollement may influence the mechanical behavior of the connecting Hunter Mountain fault. Perhaps listric motion on the Panamint Valley fault also promotes nascent metamorphic core complex formation and shallowing of the brittle-ductile transition.

Long-term fault slip rate estimates based on geodetic data can be sensitive to earthquake cycle effects and assumed crustal rheology, which affect the pattern of strain accumulation near the fault (Dixon et al., 2003). However, the high velocity gradient we observe across the Hunter Mountain fault with InSAR, and implied shallow locking depth, means that the slip rate estimate is not sensitive to details of the rheological model. Our estimate of the slip rate of the Hunter Mountain fault is based on the assumption that the fault moves only horizontally. GPS vector data 30 km to the south, across the Panamint Valley–Ash Hill fault zone, provide an opportunity to test this and other assumptions in the InSAR-based rate estimate. Here, we observe

Table 1
Average low misfit solution for viscoelastic models of Schmalzle (2008), profiles 50–120. Profiles location is indicated by dashed lines on Fig. 1. Italicized numbers are varied for best fit.

	Rate (mm/yr)	Earthquake Recurrence (yrs)	Last Earthquake (yr A.D.)
Owens Valley Fault	*0.96*	*1955*	1870[a]
Panamint Valley Fault	*5.14*	500[b]	*1841*
Death Valley Fault	*2.88*	1000[c]	*1619*
San Andreas Fault	36.00[d]	200[d]	1857[d]

[a] Date of last earthquake on Owens Valley fault.
[b] Oswald and Wesnousky (2002).
[c] Klinger and Sarna-Wojcicki (2001).
[d] Schmalzle et al. (2006).

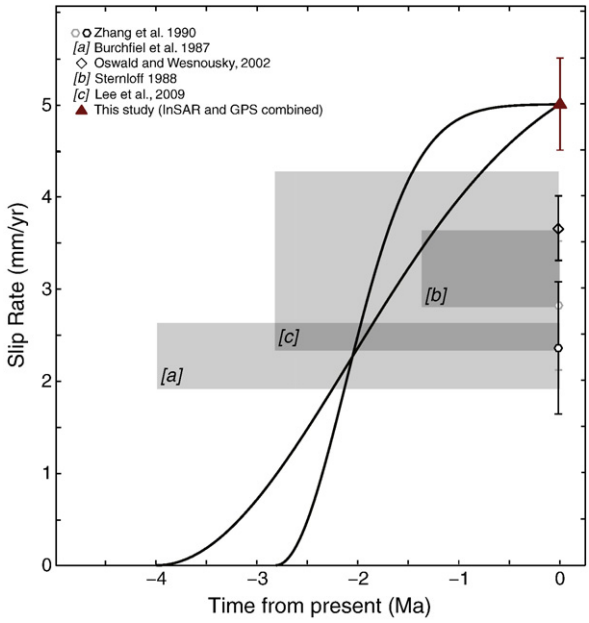

Fig. 5. Rate estimates for the Hunter Mountain–Panamint Valley fault for various time periods, and corresponding growth models. Estimated uncertainty shown by error bars or vertical box dimensions. Light gray (Zhang et al., 1990) symbol is obtained by projecting horizontal slip rate of the Panamint Valley segment onto the Hunter Mountain fault; note that the Ash Hill fault is not included here because its relation with the Panamint Valley fault is unclear and because its slip rate of 0.3 mm/yr over the last 4 Ma (Densmore and Anderson, 1997) does not impact on our conclusions. Shaded rectangles represent geologic rate and uncertainty (vertical axis) and age range of the rate estimate (horizontal axis); a) based on 9.3 ± 1.4 km offset and post 4.0 Ma faulting (Burchfiel et al. 1987, Hodges et al. 1989, Sternloff, 1988); b) based on Saline Valley reconstruction with 4.6 km of post-1.4 Ma offset (Sternloff, 1988); c) based on Lee et al. (2009). Curves show two possible Rayleigh models yielding total offset of 9.3 km: Beginning at 4 Ma (Burchfiel et al. 1987, Hodges et al. 1989) (S equals 1.9 Ma); Beginning at 2.8 Ma (Lee et al. 2009) (S equals 0.7 Ma).

more typical locking depths (10–20 km) and the slip rate we obtain is sensitive to the details of the rheological model.

7. Hunter Mountain Fault slip evolution

A simple model of constant slip rate since the time of initiation at 2.8 Ma, and satisfying the present day slip rate of 5 mm/yr would lead to a total fault offset of 14 km, significantly higher than the mapped value of 9.3 ± 1.4 km.

A simple model involving a linear increase in slip rate through time from zero to 5.0 mm/yr at present (our new geodetic result), predicts the correct total offset of 9.3 km if the fault initiates at 3.7 Ma; the inferred acceleration in slip rate is ~1.3 mm/yr per million years. However, this model is not consistent with the younger (2.8 Ma) age for fault initiation (Lee et al., 2009); for a fault beginning at zero rate at this younger time, increasing linearly to the present rate of 5.0 mm/yr, total offset is 7.0 km, significantly less than the mapped value, 9.3 ± 1.4 km.

We suggest that the Hunter Mountain–Panamint Valley fault zone illustrates the process of fault acceleration and simplification. Figure 5 shows two growth curves following a Rayleigh distribution for the Hunter Mountain fault that bracket the range of plausible values for inception time and are consistent with the measured geodetic rate. Both give total offset of 9.3 km. For the 2.8 Ma inception time (our preferred model), D_s is ~0.5 km. Faults with offset much less than this can be considered immature, while faults with offset much more than this can be considered mature. By this definition, the Hunter Mountain–Panamint Valley fault can be considered mature.

8. Discussion

While there are many possible sources of fault slip rate discrepancies, we suggest that the various rate estimates that characterize the Hunter Mountain fault over different time spans are best considered in the context of a model for a relatively young fault that is undergoing (or has recently undergone) rapid acceleration and evolution. Many authors have discussed the processes by which faults mature. As total offset increases, asperities and other frictional barriers to slip are reduced, segment length increases, en-echelon segments straighten and join, and the fault generally simplifies, reducing resistance to slip (Stirling et al., 1996; Tchalenko, 1970; Wesnousky, 1988). Ben-Zion and Sammis (2003) describe this as an inevitable consequence of strain weakening rheology, common in crustal materials. Presuming a constant tectonic driving force, as slip resistance decreases, the fault will accelerate to some steady state slip rate, and remain in that state until the tectonic driving force changes. With less than 10 km of total offset, the Hunter Mountain fault may not have achieved this mature state, or achieved it only recently. Presumably it experienced a period of geometric simplification and acceleration after 2.8 Ma.

In general, fault evolution may be considered a balance between local frictional conditions, resisting motion, and regional tectonic conditions, promoting motion. Our model simplifies this complex topic, dealing only with the initial growth phase of fault evolution, where the tendency to straighten and simplify with increasing offset lowers slip resistance; the "death" phase, associated with changing tectonics, is ignored. Many faults will never reach R_f, because of changing kinematic boundary conditions; changing plate configuration may require formation of new faults and abandonment of existing faults. Even if a mature fault reaches R_f, some distributed, off-fault deformation may still occur, unrecorded by geologic estimates of offset on the main fault trace. Perhaps this is why the Holocene rate on the Carrizo segment of the San Andreas Fault (34 mm/yr; Liu-Zeng et al., 2006) is slightly lower than the geodetic rate (36 mm/yr; Schmalzle et al., 2006). While the two values overlap within current uncertainties, future studies may show this small difference to be real.

Given rapid growth of the Hunter Mountain fault after 2.8 Ma, it is interesting to speculate concerning its influence on adjacent ECSZ faults. Our model, as well as previous studies (Stirling et al., 1996; Tchalenko, 1970; Wesnousky, 1988) predicts increasing geometric simplification of fault zones with time. Thus, it might be expected that the ECSZ will also simplify, with one fault (perhaps the Hunter Mountain–Panamint Valley fault) becoming dominant. Several authors have speculated that the ECSZ has accelerated in the last few million years, e.g., in response to the post 5.5 Ma inland jump of the Pacific–North America plate boundary, or due to post-3.5 Ma crustal delamination that led to Sierra Nevada uplift (Jones et al., 2004). In this case, the Hunter Mountain–Panamint Valley fault may have accommodated most of the acceleration.

9. Conclusions

Knowledge of a fault's total offset and initiation age, combined with an accurate estimate of the present-day rate from geodesy, yield useful constraints on fault growth and evolution. For the Hunter Mountain–Panamint Valley fault, available geologic data (fault inception time between 4 and 2.8 Ma, total offset of 9.3 km) and geodetic data (present day rate of 5.0 ± 0.5 mm/yr) are satisfied with a simple model of fault acceleration and evolution. In this accelerating fault model, the geodetic rate estimate is invariably faster than long-term geologic rate estimates.

Acknowledgments

This work was supported by a NASA (NNG05GP80H) fellowship and Fritz Koczy fellowship to N.G., NSF grants to T.H.D and F.A. and an NSF

(0847985) and NASA (NNG05GA83H) fellowship to G.S. We thank Jeff Lee for making available his geochronology data in advance of publication, Christopher Harrison for suggesting use of the Rayleigh cumulative distribution, and Kurt Frankel for a thorough review. UNAVCO, Winsar, GeoEarthsope and ESA generously provided data for this study. Steve Wesnousky, Dan Stockli, Sarah Roeske and Mike Ortiz provided very useful comments on an earlier version of this paper.

References

Atwater, T.M., 1989. Plate Tectonic History of the Northeast Pacific and Western North America. In: Winterer, E.L., Hussong, D.M., Decker, R.W. (Eds.), The geology of North America, v. N; The northeastern Pacific Ocean and Hawaii. Geol. Soc. Amer, Boulder, CO, pp. 21–72.

Atwater, T., Stock, J., 1998. Pacific North America plate tectonics of the Neogene southwestern United States: an update. Int. Geol. Rev. 40, 375–402.

Bell, J.W., Caskey, S.J., Ramelli, A.R., Guerrieri, L., 2004. Pattern and rates of faulting in the central Nevada seismic belt, and paleoseismic evidence for prior beltlike behavior. Bull. Seismol. Soc. Am. 94, 1229–1254.

Bennett, R.A., Reilinger, R.E., Rodi, W., Li, Y., Toksöz, M.N., Hudnut, K., 1995. Coseismic fault slip associated with the 1992 M w 6.1 Joshua Tree, California, earthquake: implications for the Joshua Tree-Landers earthquake sequence. J. Geophys. Res. 100, 6443–6461.

Bennett, R.A., Wernicke, B.P., Niemi, N.A., Friedrich, A.M., Davis, J.L., 2003. Contemporary strain rates in the northern Basin and Range province from GPS data. Tectonics 22.

Bennett, R.A., Friedrich, A.M., Furlong, K.P., 2004. Codependent histories of the San Andreas and San Jacinto fault zones from inversion of fault displacement rates. Geology 32, 961–964.

Ben-Zion, Y., Sammis, C.G., 2003. Characterization of fault zones. Pure Appl. Geophys. 160, 677–715.

Berardino, P., Fornaro, G., Lanari, R., Sansosti, E., 2002. A new algorithm for surface deformation monitoring based on small baseline differential SAR interferograms. IEEE Trans. Geosci. Remote Sens. 40, 2375–2383.

Bodin, P., Bilham, R., Behr, J., Gomberg, J., Hudnut, K.W., 1994. Slip triggered on Southern California Faults by the 1992 Joshua-Tree, Landers, and Big-Bear Earthquakes. Bull. Seismol. Soc. Am. 84, 806–816.

Brooks, B.A., Frazer, L.N., 2005. Importance reweighting reduces dependence on temperature in Gibbs samplers: an application to the coseismic geodetic inverse problem. Geophys. J. Int. 161, 12–20.

Burchfiel, B.C., Hodges, K.V., Royden, L.H., 1987. Geology of Panamint Valley–Saline Valley pull-apart system, California–Palinspastic evidence for low-angle geometry of a neogene range-bounding fault. J. Geophys. Res. Sol. Earth Planet. 92, 10422–10426.

Calzia, J.P., Ramo, O.T., 2000. Late Cenozoic crustal extension and magmatism, southern Death Valley region, California: Great Basin and Sierra Nevada, 2, pp. 135–164.

DeMets, C., Dixon, T.H., 1999. New kinematic models for Pacific–North America motion from 3 Ma to present, I: Evidence for steady motion and biases in the NUVEL-1A model. Geophys. Res. Lett. 26, 1921–1924.

Densmore, A.L., Anderson, R.S., 1997. Tectonic geomorphology of the Ash Hill fault, Panamint Valley, California. Basin Res. 9, 53–63.

Dickinson, W.R., 1996. Kinematics of transrotational tectonism in the California Transverse Ranges and its contribution to the cumulative slip along the San Andreas transform fault system. Geol. Soc. Am. Spec. Pap. 305, 46.

Dixon, T.H., Robaudo, S., Lee, J., Reheis, M.C., 1995. Constraints on present-day basin and range deformation from space geodesy. Tectonics 14, 755–772.

Dixon, T., Farina, F., DeMets, C., Suarez-Vidal, F., Fletcher, J., Marquez-Azua, B., Miller, M., Sanchez, O., Umhoefer, P., 2000. New kinematic models for Pacific-North America motion from 3 ma to present, II: Evidence for a “Baja California shear zone”. Geophys. Res. Lett. 27, 3961–3964.

Dixon, T.H., Norabuena, E., Hotaling, L., 2003. Paleoseismology and global positioning system: earthquake-cycle effects and geodetic versus geologic fault slip rates in the Eastern California shear zone. Geology 31, 55–58.

Dokka, R.K., Travis, C.J., 1990a. Late Cenozoic strike-slip faulting in the Mojave Desert, California. Tectonics 9, 311–340.

Dokka, R.K., Travis, C.J., 1990b. Role of the Eastern California shear zone in accommodating Pacific–North-American plate motion. Geophys. Res. Lett. 17, 1323–1326.

Dolan, J.F., Bowman, D.D., Sammis, C.G., 2007. Long-range and long-term fault interactions in Southern California. Geology 35, 855–858.

Du, Y.J., Aydin, A., 1996. Is the San Andreas big bend responsible for the Landers earthquake and the eastern California shear zone? Geology 24, 219–222.

Fialko, Y., 2006. Interseismic strain accumulation and the earthquake potential on the southern San Andreas fault system. Nature 441, 968–971.

Fialko, Y., Sandwell, D., Simons, M., Rosen, P., 2005. Three-dimensional deformation caused by the Bam, Iran, earthquake and the origin of shallow slip deficit. Nature 435, 295–299.

Frankel, K.L., Brantley, K.S., Dolan, J.F., Finkel, R.C., Klinger, R.E., Knott, J.R., Machette, M.N., Owen, L.A., Phillips, F.M., Slate, J.L., Wernicke, B.P., 2007. Cosmogenic 10Be and 36Cl geochronology of offset alluvial fans along the northern Death Valley fault zone: implications for transient strain in the eastern California shear zone. J. Geophys. Res. 112, B06407.

Friedrich, A.M., Lee, J., Wernicke, B.P., Sieh, K., 2004. Geologic context of geodetic data across a Basin and Range normal fault, Crescent Valley, Nevada. Tectonics 23.

Gourmelen, N., Amelung, F., 2005. Postseismic mantle relaxation in the Central Nevada Seismic Belt. Science 310, 1473–1476.

Gourmelen, N., Amelung, F., Casu, F., Manzo, M., Lanari, R., 2007. Mining-related ground deformation in Crescent Valley, Nevada: implications for sparse GPS networks. Geophys. Res. Lett. 34, L09309.

Gourmelen, N., Amelung, F., Lanari, R., 2010. Interferometric synthetic aperture radar–GPS integration: interseismic strain accumulation across the Hunter Mountain fault in the eastern California shear zone. J. Geophys. Res. 115, B09408.

Guest, B., Niemi, N., Wernicke, B., 2007. Stateline fault system: a new component of the Miocene–Quaternary Eastern California shear zone. Geol. Soc. Am. Bull. 119, 1337–1347.

Hodges, K.V., Mckenna, L.W., Stock, J., Knapp, J., Page, L., Sternlof, K., Silverberg, D., Wust, G., Walker, J.D., 1989. Evolution of extensional basins and basin and range topography west of Death-Valley, California. Tectonics 8, 453.

Johnson, K.M., Hilley, G.E., Burgmann, R., 2007. Influence of lithosphere viscosity structure on estimates of fault slip rate in the Mojave region of the San Andreas fault system. J. Geophys. Res. Solid Earth 112.

Jones, C.H., Farmer, G.L., Unruh, J., 2004. Tectonics of Pliocene removal of lithosphere of the Sierra Nevada, California. Geol. Soc. Am. Bull. 116, 1408–1422.

Klinger, R.E., Sarna-Wojcicki, A.M., 2001. Field trip guide for Day A, northern Death Valley. 01-51.

Kurth, R.E., Cox, D.C., 1985. Discrete probability-distributions for probabilistic fracture-mechanics. Risk Anal. 5, 235–240.

Lanari, R., Mora, O., Manunta, M., Mallorqui, J.J., Berardino, P., Sansosti, E., 2004. A small-baseline approach for investigating deformations on full-resolution differential SAR interferograms. IEEE Trans. Geosci. Remote Sens. 42, 1377–1386.

Lee, J., Spencer, J., Owen, L., 2001. Holocene slip rates along the Owens Valley Fault, California: implications for the recent evolution of the Eastern California Shear Zone. Geology 29, 819–822.

Lee, J., Stockli, D.F., Owen, L.A., Finkel, R.C., Kislitsyn, R., 2009. Exhumation of the Inyo Mountains, California: implications for the timing of extension along the western boundary of the Basin and Range Province and distribution of dextral fault slip rates across the eastern California shear zone. Tectonics 28.

Lisowski, M., Savage, J.C., Prescott, W.H., 1991. The velocity-field along the San-Andreas fault in Central and Southern California. J. Geophys. Res. Sol Earth Planet. 96, 8369–8389.

Liu, J., Sieh, K., Hauksson, E., 2003. A structural interpretation of the aftershock “Cloud” of the 1992 M-w 7.3 Landers earthquake. Bull. Seismol. Soc. Am. 93, 1333–1344.

Liu-Zeng, J., Klinger, Y., Sieh, K., Rubin, C., Seitz, G., 2006. Serial ruptures of the San Andreas fault, Carrizo Plain, California, revealed by three-dimensional excavations. J. Geophys. Res. Solid Earth 111.

Lundgren, P., Usai, S., Sansosti, E., Lanari, R., Tesauro, M., Fornaro, G., Berardino, P., 2001. Modeling surface deformation observed with synthetic aperture radar interferometry at Campi Flegrei caldera. J. Geophys. Res. Solid Earth 106, 19355–19366.

Marco, S., Stein, M., Agnon, A., Ron, H., 1996. Long-term earthquake clustering: a 50,000-year paleoseismic record in the Dead Sea Graben. J. Geophys. Res. Solid Earth 101, 6179–6191.

Massonnet, D., Rossi, M., Carmona, C., Adragna, F., Peltzer, G., Feigl, K., Rabaute, T., 1993. The displacement field of the Landers earthquake mapped by radar interferometry. Nature 364, 138–142.

McClusky, S.C., Bjornstad, S.C., Hager, B.H., King, R.W., Meade, B.J., Miller, M.M., Monastero, F.C., Souter, B.J., 2001. Present day kinematics of the Eastern California Shear Zone from a geodetically constrained block model. Geophys. Res. Lett. 28, 3369–3372.

McQuarrie, N., Wernicke, B.P., 2005. An animated tectonic reconstruction of southwestern North America since 36 Ma. An animated tectonic reconstruction of Southwestern North America since 36 Ma. Geosphere 1, 147–172.

Meade, B.J., Hager, B.H., 2005. Block models of crustal motion in southern California constrained by GPS measurements. J. Geophys. Res. Solid Earth 110.

Miller, M.M., Johnson, D.J., Dixon, T.H., Dokka, R.K., 2001. Refined kinematics of the Eastern California shear zone from GPS observations, 1993–1998. J. Geophys. Res. Solid Earth 106, 2245–2263.

Monastero, F.C., Katzenstein, A.M., Miller, J.S., Unruh, J.R., Adams, M.C., Richards-Dinger, K., 2005. The Coso geothermal field: a nascent metamorphic core complex. Geol. Soc. Am. Bull. 117, 1534–1553.

Oskin, M., Iriondo, A., 2004. Large-magnitude transient strain accumulation on the Blackwater fault, Eastern California shear zone. Geology 32, 313–316.

Oskin, M., Stock, J., Martin-Barajas, A., 2001. Rapid localization of Pacific–North America plate motion in the Gulf of California. Geology 29, 459–462.

Oskin, M., Perg, L., Shelef, E., Strane, M., Gurney, E., Singer, B., Zhang, X., 2008. Elevated shear zone loading rate during an earthquake cluster in eastern California. Geology 36, 507–510.

Oswald, J.A., Wesnousky, S.G., 2002. Neotectonics and Quaternary geology of the Hunter Mountain fault zone and Saline Valley region, southeastern California. Geomorphology 42, 255–278.

Peltzer, G., Rosen, P., 1995. Surface displacements of the 17 May 1993 Eureka Valley, California, earthquake observed by SAR interferometry. Science 268, 1333–1336.

Peltzer, G., Crampe, F., Hensley, S., Rosen, P., 2001. Transient strain accumulation and fault interaction in the Eastern California shear zone. Geology 29, 975–978.

Reheis, C., Sawyer, T.L., 1997. Late Cenozoic history and slip rates of the Fish Lake Valley, Emigrant Peak, and Deep Springs fault zones, Nevada and California. Geol. Soc. Am. Bull. 109, 280–299.

Rockwell, T.K., Lindvall, S., Herzberg, M., Murbach, D., Dawson, T., Berger, G., 2000. Paleoseismology of the Johnson Valley, Kickapoo, and Homestead Valley Faults: clustering of Earthquakes in the Eastern California Shear Zone. Bull. Seismol. Soc. Am. 90, 1200–1236.

Sauber, J., Thatcher, W., Solomon, S.C., Lisowski, M., 1994. Geodetic slip rate for the Eastern California shear zone and the recurrence time of Mojave Desert earthquakes. Nature 367, 264–266.

Savage, J.C., Burford, R.O., 1973. Geodetic Determination of Relative Plate Motion in Central California. J. Geophys. Res. 78, 832–845.
Savage, J.C., Lisowski, M., 1998. Viscoelastic coupling model of the San Andreas Fault along the big bend, southern California. J. Geophys. Res. Solid Earth 103, 7281–7292.
Savage, J.C., Lisowski, M., Prescott, W.H., 1990. An apparent shear zone trending North–Northwest across the Mojave-Desert into Owens-Valley, Eastern California. Geophys. Res. Lett. 17, 2113–2116.
Schmalzle, G., 2008. The Earthquake Cycle of Strike-Slip Faults, PhD thesis, Univ. of Miami, Miami.
Schmalzle, G., Dixon, T., Malservisi, R., Govers, R., 2006. Strain accumulation across the Carrizo segment of the San Andreas Fault, California: impact of laterally varying crustal properties. J. Geophys. Res. Solid Earth 111.
Sella, G.F., Dixon, T.H., Mao, A.L., 2002. REVEL: a model for recent plate velocities from space geodesy. J. Geophys. Res. Solid Earth 107.
Sieh, K.E., Jahns, R.H., 1984. Holocene activity of the San-Andreas fault at Wallace-Creek, California. Geol. Soc. Am. Bull. 95, 883–896.
Sternloff, K. R., 1988. Structural style and kinematic history of the active Panamint-Saline extensional system, Inyo county, California. PhD, 30.
Stirling, M.W., Wesnousky, S.G., Shimazaki, K., 1996. Fault trace complexity, cumulative slip, and the shape of the magnitude-frequency distribution for strike-slip faults: a global survey (vol. 124, pg 833, 1996). Geophys. J. Int. 126, 301.
Stockli, D.F., Dumitru, T.A., McWilliams, M.O., Farley, K.A., 2003. Cenozoic tectonic evolution of the White Mountains, California and Nevada. Bull. Geol. Soc. Am. 115, 788–816.
Tchalenko, J.S., 1970. Similarities between shear zones of different magnitudes. Geol. Soc. Am. Bull. 81, 1625–1640.
U.S. Geological Survey, New Mexico Bureau of Mines and Mineral Resources and Nevada Bureau of Mines and Geology, 2006. Quaternary Fault and Fold Database for the United States. 2010.
Walker, J.D., Kirby, E., Andrew, J.E., 2005. Strain transfer and partitioning between the Panamint Valley, Searles Valley, and Ash Hill fault zones, California. Geosphere 1, 111–118.
Ward, S.N., 1990. Pacific–North America plate motions: new results from very long baseline interferometry. J. Geophys. Res. 95, 21,965–21,981.
Weertman, J., Weertman, J.R., 1964. Elementary Dislocation Theory. Macmillan, New York.
Wernicke, B., Snow, J.K., 1998. Cenozoic tectonism in the central basin and range: motion of the Sierran Great Valley block. Int. Geol. Rev. 40, 403–410.
Wesnousky, S.G., 1988. Seismological and structural evolution of strike-slip faults. Nature 335, 340–342.
Zechar, J.D., Frankel, K.L., 2009. Incorporating and reporting uncertainties in fault slip rates. J. Geophys. Res. 114, B12407.
Zhang, P.Z., Ellis, M., Slemmons, D.B., Mao, F.Y., 1990. Right-lateral displacements and the Holocene slip rate associated with prehistoric earthquakes along the Southern Panamint Valley Fault Zone — implications for southern basin and range tectonics and coastal California deformation. J. Geophys. Res. 95, 4857–4872.